Supplementary Material Section

Impact of disorder on the optoelectronic properties of $GaN_yAs_{1-x-y}Bi_x$ alloys and heterostructures

Muhammad Usman[1], Christopher A. Broderick[2,3], Eoin P. O'Reilly[2,4]

[1] *School of Physics, The University of Melbourne, Parkville, 3010, Victoria Australia*

[2] *Tyndall National Institute, Lee Maltings, Dyke Parade, Cork T12 R5CP, Ireland*

[3] *Department of Electrical and Electronic Engineering, University of Bristol, Bristol BS8 1UB, U.K.*

[4] *Department of Physics, University College Cork, Cork T12 YN60, Ireland*

Section S1: Theoretical Models

The unusual electronic properties of dilute nitride and bismide alloys derive from the fact that, when incorporated in dilute concentrations, N and Bi act as isovalent impurities which strongly perturb the band structure of the host matrix semiconductor. [16, 21, 38] As a result, the details of electronic structure are strongly influenced, even at dilute compositions, by short-range alloy disorder [16, 23, 26, 33] – i.e. the formation of pairs and larger clusters of N and Bi atoms sharing common cation nearest neighbours – meaning that highly-mismatched alloys pose significant challenges for theory. Firstly, due to the prominence of impurity effects conventional approaches to analyse alloy band structures, such as the virtual crystal approximation, break down. Secondly, since the effects of Bi and N incorporation are prominent at dilute compositions and in the presence of alloy disorder, quantitative understanding of the properties of real materials must be built on analysis of systems containing upwards of thousands of atoms: [16, 28, 34, 39] the minimum N or Bi composition that can be considered using a $2M$-atom $Ga_MAs_{M-1}X_1$ (X = N, Bi) supercell is M^{-1}. For example, to consider an alloy composition of 0.1% then requires a supercell containing a minimum of 2000 atoms ($M^{-1} = 10^{-3}$) and, since a 2000-atom supercell corresponds only to a

single substitutional impurity, there is no scope to investigate disorder effects unless the system size is significantly increased.

These features generally place the study of highly-mismatched alloys beyond the reach of contemporary first principles methods, since sufficiently advanced approaches cannot be applied *directly* to such large systems due to their associated computational expense. This then mandates the development of alternative theoretical approaches. Indeed, while first principles analyses have provided valuable insights and information, detailed understanding of the properties of real dilute nitride and bismide alloys has to date primarily been built via the development and application of appropriate semi-empirical pseudopotential [14–16, 39] and tight-binding (TB) [6, 23, 26, 28, 30, 34] models. Further analysis has shown that simple continuum models – derived and parametrised on the basis of either (i) experimental measurements, [1, 29] or (ii) electronic structure calculations [7, 28] – provide an effective means to understand and analyse the main features of the band structure of N- and Bi-containing alloys, by describing general trends in important material parameters (despite omitting the detailed features of the electronic structure). Here, in the following two sections, we present two models of the electronic structure of $GaN_yAs_{1-x-y}Bi_x$ alloys: (i) an atomistic sp^3s^* TB model, and (ii) a continuum, extended basis set 14-band **k·p** Hamiltonian.

Section S1.A: Atomistic Tight-binding Model

Since the TB method employs a basis set of localised atomic orbitals, it is ideally suited to probe the electronic structure of localised impurities. [25] This, combined with its low computational cost, means that appropriately parametrised TB models provide a physically transparent and highly effective means by which to systematically analyse the properties of large, disordered systems. We have previously demonstrated that the TB method provides a detailed understanding of the electronic and optical properties of GaN_yAs_{1-y} and $GaAs_{1-x}Bi_x$ alloys, and that the results of calculations based on this approach are in quantitative agreement with a wide range of experimental data. [6, 23, 27, 33, 34] Here, we extend this approach to quaternary $GaN_yAs_{1-x-y}Bi_x$ alloys.

To accurately describe states lying close in energy to the VB and CB edges we employ an sp^3s^* basis set, [36] thereby allowing the dispersion of the lowest CB to be described throughout the entire Brillouin zone without explicit introduction of d orbitals, which avoids significant parametric complexity. Our TB parameters for the band structures of the GaN, GaAs and GaBi compounds

are obtained on the basis of first principles band structure calculations. [12, 34] Spin-orbit coupling between p orbitals is included explicitly in the model, in order to account for the known, strong relativistic effects associated with Bi incorporation in (In)GaAs. [2, 11, 34] To construct alloy supercells we replace As atoms by N or Bi atoms at selected positions on the anion sublattice. To account for the important effects [16, 22, 34, 39] of lattice relaxation about N and Bi lattice sites, the relaxed atomic positions in a given supercell are determined by minimising the total elastic energy using a valence force field (VFF) model, based on the Keating potential and including anharmonic corrections to account accurately for the large local strains arising due to the significant differences in the covalent radii of N, As and Bi. [13, 19, 34]

In our TB model the atomic orbital energies for a given atom are taken to depend on the local neighbour environment by (i) averaging over the orbital energies of the compounds formed by the atom and each of its nearest neighbours, and (ii) renormalising the nearest-neighbour averaged orbital energy obtained in this manner to account firstly for the mixed-anion local environment (seen by a cation having nearest neighbour anions of different atomic species) and, secondly, for the non-local nature of the lattice relaxation brought about by the aforementioned large differences in the anion covalent radii. In this approach the energy of orbital α ($= s, p_x, p_y, p_z, s^*$) in the atom located at lattice site n ($= 1, \ldots, 2M$) is given by [20]

$$E_{n\alpha} = \frac{1}{4}\sum_j \Bigg[\underbrace{\Delta E_{\rm VB}(nj) + E_\alpha(nj)}_{\text{Nearest-neighbour bond}} + \underbrace{\sum_{k\neq j}\left(\frac{\Delta E_\alpha}{\Delta d_0}\right)_{njk}\Big(d(jk) - d_0(jk)\Big)}_{\text{Mixed anion local environment}} + \underbrace{\left(\frac{\sum_{\rm X} M_{\rm X}\left(\frac{\Delta E_\alpha}{\Delta d_0}\right)_{\rm GaAsX}}{\sum_{\rm X} M_{\rm X}}\right)\Big(d(nj) - d_0(nj)\Big)}_{\text{Non-local lattice relaxation}} \Bigg], \tag{S1}$$

where X = N or Bi, and the sum runs over the four nearest neighbours j of atom n. $E_\alpha(nj)$, $\Delta E_{\rm VB}(nj)$ and $d_0(nj)$ respectively denote the energy of orbital α, the VB offset, and the unstrained nearest-neighbour bond length of the compound formed by atoms n and j. $d(nj)$ is the relaxed bond length between atoms n and j in the supercell, $M_{\rm X}$ is the total number of N *or* Bi atoms, and $\sum_{\rm X} M_{\rm X}$ is the total number of N *and* Bi atoms. The magnitude of the second and third terms in Eq. (S1) is determined by [20]

$$\left(\frac{\Delta E_\alpha}{\Delta d_0}\right)_{njk} = \frac{E_\alpha(nj) - E_\alpha(nk)}{d_0(nj) - d_0(nk)}, \tag{S2}$$

which is the ratio of the difference between the energy of orbital α to that between the equilibrium bond lengths, for the compounds formed by atom n and its nearest neighbours j and k (with E_α assumed here to include the corresponding VB offset ΔE_{VB} for a given compound).

The first term in Eq. (S1) describes conventional averaging of the orbital energy over nearest-neighbours. The second and third terms in Eq. (S1) describe a renormalisation of the orbital energy, and respectively account for (i) the large, bond length dependent differences between the orbital energies in the compounds formed by a given atom and nearest neighbours of differing atomic species, and (ii) the relaxation of the crystal lattice in response to substitutional incorporation of an impurity X atom. Previous analysis [20, 24] has shown that it is pertinent to include an orbital energy renormalisation of this form to account for the fact that substitutional N and Bi atoms have significant differences in electronegativity and covalent radii compared to the As atoms they replace, meaning that they perturb the structural and electronic properties much more severely than in conventional III-V alloys.

The nature of the orbital energy renormalisation is best understood by considering its action in the presence of an isolated substitutional impurity. In a $\mathrm{Ga}_M\mathrm{As}_{M-1}\mathrm{X}_1$ supercell a cation (Ga atom) having the X atom as a nearest neighbour sits in a mixed-anion nearest-neighbour environment (formed by the X atom and three As atoms). Due to relaxation of the crystal lattice, the length of the Ga-X bond is smaller (larger) than the three Ga-As nearest-neighbour bonds when X = N (Bi). [16, 34] The second term in Eq. (S1) proceeds in a pairwise manner, adjusting the contribution of a given nearest-neighbour bond to the Ga orbital energy by accounting for the large differences in Ga orbital energies between GaAs and GaX – i.e. between those in compounds formed by the Ga atom and its X or As nearest neighbours. For a given nearest-neighbour bond the magnitude of the renormalisation term is determined by the multiplicative factor $d(jk) - d_0(jk)$, which is non-zero only when the relaxed bond length differs from $d_0(jk)$, thus describing a simple linear variation of the Ga orbital energy with bond length in going from GaAs to GaX.

The relaxation of the crystal lattice about the X atomic site generally propagates through the crystal on a length scale which exceeds typical nearest-neighbour bond lengths. However, by definition the action of the second term in Eq. (S1) is explicitly limited to nearest neighbours: the As second-nearest neighbours of the X atom in a $\mathrm{Ga}_M\mathrm{As}_{M-1}\mathrm{X}_1$ supercell ($M_{\mathrm{X}} = \sum_{\mathrm{X}} M_{\mathrm{X}} = 1$) have four Ga nearest neighbours, in which case the factor defined by Eq. (S2) vanishes, despite that the relaxed second-nearest neighbour bond lengths will be different from those in unstrained GaAs. This non-local perturbation of the crystal structure is taken into account by the third term

TABLE S1. Band structure parameters for the constituent compounds in the sp^3s^* tight-binding model of $GaN_yAs_{1-x-y}Bi_x$, including the valence band offsets ΔE_{VB}, orbital energies E_α ($\alpha = s, p$ and s^*), inter-atomic interaction matrix elements V_δ ($\delta = ss\sigma$, $pp\sigma$, $pp\pi$, $s_cp_a\sigma$, $s_ap_c\sigma$, $s_c^*p_a\sigma$ and $s_a^*p_c\sigma$), and renormalised atomic spin-orbit splitting energies $\Delta_{c,a}$. All parameters are given in units of eV.

Parameter	GaN	GaAs	GaBi
ΔE_{VB}	−2.28	0.00	1.10
E_{s_c}	−0.9994	−2.9474	−5.6126
E_{s_a}	−12.3306	−8.6336	−8.3774
E_{p_c}	8.5803	3.5532	1.6940
E_{p_a}	−2.7197	0.9252	−0.1256
$E_{s_c^*}$	12.2000	6.2000	5.8164
$E_{s_a^*}$	12.2000	7.0914	6.1262
$V_{ss\sigma}$	−2.0700	−1.6835	−1.3425
$V_{pp\sigma}$	5.0530	2.9500	2.0003
$V_{pp\pi}$	−0.7150	−0.7420	−0.6345
$V_{s_cp_a\sigma}$	3.0593	2.4200	1.2025
$V_{s_ap_c\sigma}$	2.0717	2.3920	2.3567
$V_{s_c^*p_a\sigma}$	2.8375	2.0400	0.5100
$V_{s_a^*p_c\sigma}$	1.5442	1.7700	1.8051
Δ_c	0.0020	0.1350	0.6714
Δ_a	0.0070	0.0550	0.0384

in Eq. (S1), which renormalises the orbital energy via a weighted average of the ratio defined in Eq. (S2) over all substitutional impurities in the supercell. The magnitude of this correction is again determined by the difference between the relaxed and unstrained nearest-neighbour bond lengths, meaning that (i) it applies at all atomic sites that have been affected by the lattice relaxation, and (ii) its magnitude decreases as the distance from the X atomic site increases, in line with the magnitude of the lattice relaxation.

This orbital energy renormalisation therefore provides a suitable manner by which to explicitly incorporate the non-local nature of the perturbation to the supercell Hamiltonian – associated with N and/or Bi incorporation – into what is implicitly a nearest-neighbour model. Also, since this

TABLE S2. Dimensionless exponents η_δ ($\delta = ss\sigma$, $pp\sigma$, $pp\pi$, $s_c p_a\sigma$, $s_a p_c\sigma$, $s_c^* p_a\sigma$ and $s_a^* p_c\sigma$) used to rescale the inter-atomic interaction matrix elements V_δ for the constituent compounds in the sp^3s^* tight-binding model of $GaN_yAs_{1-x-y}Bi_x$ (cf. Eq. (S3)).

Parameter	GaN	GaAs	GaBi
$\eta_{ss\sigma}$	3.030	3.512	3.660
$\eta_{pp\sigma}$	2.090	3.204	2.200
$\eta_{pp\pi}$	3.720	4.326	3.240
$\eta_{s_c p_a\sigma}$	3.500	4.500	4.090
$\eta_{s_a p_c\sigma}$	4.000	4.100	4.080
$\eta_{s_c^* p_a\sigma}$	6.200	7.200	7.200
$\eta_{s_a^* p_c\sigma}$	4.000	4.200	4.200

TABLE S3. Unstrained bond lengths (d_0), and bond stretching (α) and bond-angle bending (β) force constants for the constituent compounds in the valence force field potential used to relax the atomic positions in $GaN_yAs_{1-x-y}Bi_x$ supercells.

Parameter	GaN	GaAs	GaBi
d_0 (Å)	1.944	2.448	2.740
α (N m^{-1})	158.00	41.18	61.00
β (N m^{-1})	14.66	8.95	6.21

approach relies only on the known atomic orbital energies and nearest-neighbour bond lengths, it has the benefit of circumventing the need to introduce additional parameters to describe these important beyond-nearest-neighbour effects.

The inter-atomic interaction matrix elements between a given pair of nearest neighbour atoms are computed in the model by (i) using the two-centre integrals of Slater and Koster [31] to take into account changes in bond angle, and (ii) incorporating a bond length dependent rescaling to account for the difference between the relaxed bond length between a pair of neighbouring atoms in the supercell, and the equilibrium bond length of the compound formed by the same two atoms. For each distinct type of interaction, the bond length dependent rescaling of the interaction matrix element between nearest neighbours n and j is given by

$$V_\delta(d(nj)) = V_\delta(nj)\left(\frac{d_0(nj)}{d(nj)}\right)^{\eta_\delta}, \tag{S3}$$

where $V_\delta(nj)$ is the corresponding interaction matrix element in the unstrained compound formed by atoms n and j, and $\delta = ss\sigma$, $pp\sigma$, $pp\pi$, $s_cp_a\sigma$, $s_ap_c\sigma$, $s_c^*p_a\sigma$ or $s_a^*p_c\sigma$ describes the symmetry of the interaction (with c and a denoting cations and anions, respectively). The exponent η_δ takes a distinct value for each δ – the full set are determined for each compound by fitting to the hydrostatic deformation potentials obtained from first principles calculations. [27]

In the TB method we compute the momentum matrix element between the supercell eigenstates $|n\mathbf{k}\sigma\rangle$ and $|m\mathbf{k}\sigma'\rangle$, at wave vector $\mathbf{k}$ and having spins σ and σ', in the position basis as

$$\begin{aligned} P_{nm}^{(\widehat{e})}(\mathbf{k}) &= -\frac{im_0}{\hbar}\sum_{\sigma,\sigma'}\langle n\mathbf{k}\sigma|\left[\widehat{(\widehat{e}\cdot\mathbf{r})},\widehat{H}\right]|m\mathbf{k}\sigma'\rangle \\ &= -\frac{im_0}{\hbar}\sum_{\sigma,\sigma'}\sum_{p,q}\sum_{\alpha,\beta} a^*_{np\alpha\sigma}(\mathbf{k})a_{mq\beta\sigma'}(\mathbf{k})\left(\widehat{e}\cdot\mathbf{r}_p - \widehat{e}\cdot\mathbf{r}_q\right)\langle p\alpha\sigma|\widehat{H}|q\beta\sigma'\rangle\,, \end{aligned} \tag{S4}$$

where p and q index the atomic sites in the supercell, α and β index the atomic orbitals localised at each atomic site, and $\widehat{e}$ is a unit vector defining the direction along which the corresponding emitted/absorbed photon is polarised. The final expression for $P_{nm}^{(\widehat{e})}(\mathbf{k})$ is obtained using the spectral resolution of the position operator, $\widehat{(\widehat{e}\cdot\mathbf{r})} = \sum_{p,\alpha,\sigma}(\widehat{e}\cdot\mathbf{r}_p)\,|p\alpha\sigma\rangle\langle p\alpha\sigma|$, in addition to assuming that there is no overlap between basis states localised on different lattice sites, $\langle p\alpha\sigma|q\beta\sigma'\rangle = \delta_{pq}\delta_{\alpha\beta}\delta_{\sigma\sigma'}$ (i.e. an orthogonal TB model).

The TB model was implemented within the framework of the NEMO 3-D NanoElectronic MOdeling software, which was used to carry out the supercell calculations. [17, 18]

Section S1.B: 14-band k·p Hamiltonian

Previous analysis has shown that it is possible and useful to derive simple continuum models that describe the perturbed band structure of GaN_yAs_{1-y} and $GaAs_{1-x}Bi_x$ alloys. [7, 24, 28] Phenomenological approaches, principally the band-anticrossing (BAC) model, have originated from interpretation of spectroscopic data and atomistic electronic structure calculations, and are widely employed as a straightforward and efficient means by which to describe the evolution of the main features of the band structure (principally the band gap and band edge energies) with alloy composition, both in bulk materials and in heterostructures.

For GaN_yAs_{1-y} alloys it is well established that the evolution of the CB structure can be described by a simple 2-band BAC model, in which the extended states of the GaAs host matrix CB edge undergo a composition dependent repulsive interaction (of magnitude $\beta_N\sqrt{y}$, where β_N is the BAC coupling strength and y is the N composition) with a set of localised states associated with substitutional N impurities (having energy E_N). [27] In the case where the N-related localised states lie energetically within the host matrix CB – as is the case in $(In)GaN_yAs_{1-y}$ [27] – the composition dependence of the BAC interaction between these two sets of states results in a strong reduction of the alloy CB edge energy with increasing y. It generally established that similar behaviour is present in $GaAs_{1-x}Bi_x$: the strong reduction (increase) and composition-dependent bowing of the band gap (VB spin-orbit-splitting energy) can be described in terms of a valence band-anticrossing (VBAC) interaction between the extended states of the GaAs VB edge, and localised impurity states associated with substitutional Bi impurities, which pushes the alloy VB edge upwards in energy with increasing x. Detailed analysis has demonstrated that (i) incorporation of an isolated, substitutional N (Bi) impurity in GaAs leads to the formation of A_1 (T_2) symmetric localised impurity states, which lie energetically within – i.e. are resonant with – the GaAs CB (VB), and (ii) an appropriate 10-band (12-band) $\mathbf{k}\cdot\mathbf{p}$ Hamiltonian can be derived using an extended basis set which includes these s-like (p-like) localised states, in addition to the conventional 8-band basis defined by the GaAs zone-centre Bloch states associated with the lowest energy CB, and light-hole (LH), heavy-hole (HH), and spin-split-off (SO) hole VBs. [8] Despite their simplicity, these extended $\mathbf{k}\cdot\mathbf{p}$ models have proven to be highly effective tools for the analysis of real materials and devices. For example, theoretical models based on the 10- and 12-band models have provided significant insight into the electronic and optical [5] properties of quantum well (QW) heterostructures, and have been used as a basis for quantitative prediction and design of key properties of electrically pumped semiconductor lasers, including the optical gain and carrier recombination rates. [4]

However, formally, these (V)BAC-based models suffer from two fundamental limitations. Firstly, they consider the impact on the band structure of isolated, non-interacting impurities *only*: they are hence formally applicable only to ordered alloys, thereby limiting their ability to predict the properties of real materials (which inevitably contain some degree of alloy disorder). Secondly, uncertainty surrounding the (V)BAC parameters can lead to parametric ambiguity which further reduces the predictive capability. In practice this first issue is not a significant limitation, since it is typically found that (V)BAC models provide reasonably accurate descrip-

tions of the evolution of band properties which are not particularly sensitive to the presence of short-range alloy disorder. Instead, one must be careful in the interpretation of the results of such calculations, in the knowledge that the model will describe only band properties which are not strongly effected by N and/or Bi clustering – e.g. the band gap and band edge energies, [8] but *not* the effective masses or Landé g factors. [6] This second issue can, in certain circumstances, represent an impediment to the development and application of BAC models due to an inability to unambiguously determine a consistent set of band parameters (of which there can be many) from a given set of experimental or theoretical band structure data (which are typically few in number). We have circumvented this problem in general by developing a TB-based approach [34] that allows the matrix elements of the alloy Hamiltonian to be *directly* calculated and parametrised in a chosen basis of crystal eigenstates and which – via construction of the localised impurity states associated with substitutional N and/or Bi incorporation – allows explicit evaluation of the various contributions to each matrix element – including direct computation of the (V)BAC parameters as well as virtual crystal (conventional alloy) contributions to the band edge energies – without the usual requirement to undertake post hoc fitting to the results of experimental measurements on GaN_yAs_{1-y} or $GaAs_{1-x}Bi_x$ alloys.

Turning our attention to $GaN_yAs_{1-x-y}Bi_x$ alloys, the analysis summarised above suggests that a suitable basis set must contain a minimum of 14 bands: the spin-degenerate CB, LH, HH and SO bands of the GaAs host matrix (8 bands), the A_1-symmetric N-related localised states (of which there is one spin-degenerate set; 2 bands), and the T_2-symmetric Bi-related localised states (of which there are two spin-degenerate sets; 4 bands). TB calculations on ordered $GaN_yAs_{1-x-y}Bi_x$ supercells indicate that the respective impact of N and Bi on the CB and VB structure are decoupled from one another. As such, the $GaN_yAs_{1-x-y}Bi_x$ band structure then admits a simple interpretation in terms of perturbation of the CB and VB separately by N- and Bi-related localised states, respectively. As we demonstrate in Sec. III B of the main paper, the 14-band model defined in this manner – and parametrised directly from TB calculations – provides a simple and predictive means by which to describe the band edge energies $GaN_yAs_{1-x-y}Bi_x$ alloys, even in the presence of significant alloy disorder. Details of the derivation of the 14-band $\mathbf{k}\cdot\mathbf{p}$ model can be found in Ref. 7.

Here, we focus on the calculation of the band edge energies in pseudomorphically strained $GaN_yAs_{1-x-y}Bi_x$ alloys and QWs using the 14-band $\mathbf{k}\cdot\mathbf{p}$ Hamiltonian. At the centre of the Brillouin zone ($\mathbf{k} = 0$), and in the presence of pseudomorphic strain corresponding to growth along the (001)

direction, the 14-band Hamiltonian block diagonalises into decoupled sub-matrices describing the CB, HH, and LH and SO states. There are six such matrices in total, three of which are distinct as a result of spin degeneracy. The band edge energies are then given by the eigenvalues of the following spin-degenerate matrices [3, 7, 32]

$$H_{\mathrm{CB}} = \begin{pmatrix} E_g^{(0)} + \Delta E_{\mathrm{N}} + \delta E_{\mathrm{N}}^{\mathrm{hy}} & \beta_{\mathrm{N}}\sqrt{y} \\ \beta_{\mathrm{N}}\sqrt{y} & E_g^{(0)} + \delta E_{\mathrm{CB}}^{\mathrm{VC}} + \delta E_{\mathrm{CB}}^{\mathrm{hy}} \end{pmatrix}, \tag{S5}$$

$$H_{\mathrm{HH}} = \begin{pmatrix} \delta E_{\mathrm{VB}}^{\mathrm{VC}} + \delta E_{\mathrm{VB}}^{\mathrm{hy}} - \delta E_{\mathrm{VB}}^{\mathrm{ax}} & \beta_{\mathrm{Bi}}\sqrt{x} \\ \beta_{\mathrm{Bi}}\sqrt{x} & \Delta E_{\mathrm{Bi}} + \delta E_{\mathrm{Bi}}^{\mathrm{hy}} - \delta E_{\mathrm{Bi}}^{\mathrm{ax}} \end{pmatrix}, \tag{S6}$$

$$H_{\mathrm{LH,SO}} = \begin{pmatrix} \delta E_{\mathrm{VB}}^{\mathrm{VC}} + \delta E_{\mathrm{VB}}^{\mathrm{hy}} + \delta E_{\mathrm{VB}}^{\mathrm{ax}} & -\sqrt{2}\,\delta E_{\mathrm{VB}}^{\mathrm{ax}} & \beta_{\mathrm{Bi}}\sqrt{x} \\ -\sqrt{2}\,\delta E_{\mathrm{VB}}^{\mathrm{ax}} & -\Delta_{\mathrm{SO}}^{(0)} + \delta E_{\mathrm{SO}}^{\mathrm{VC}} + \delta E_{\mathrm{VB}}^{\mathrm{hy}} & 0 \\ \beta_{\mathrm{Bi}}\sqrt{x} & 0 & \Delta E_{\mathrm{Bi}} + \delta E_{\mathrm{Bi}}^{\mathrm{hy}} + \delta E_{\mathrm{Bi}}^{\mathrm{ax}} \end{pmatrix}, \tag{S7}$$

where $E_g^{(0)}$ and $\Delta_{\mathrm{SO}}^{(0)}$ are the band gap and VB spin-orbit splitting energy of the GaAs host matrix, and the zero of energy has been set at the (unperturbed) GaAs VB edge. These matrices can be diagonalised to provide analytical expressions for the $\mathrm{GaN}_y\mathrm{As}_{1-x-y}\mathrm{Bi}_x$ band edge energies: the lower eigenvalue of Eq. (S5) is the alloy CB edge energy, the upper eigenvalue of Eq. (S6) is the alloy HH band edge energy, and the highest and lowest eigenvalues of Eq. (S7) are, respectively, the alloy LH and SO band edge energies.

In Eqs. (S5) – (S7) ΔE_{N} (ΔE_{Bi}) denotes the energy of the N- (Bi-) related localised states relative to the unperturbed GaAs CB (VB) edge: $\Delta E_{\mathrm{N}} > 0$ (< 0) corresponds to a resonant (bound) N-related localised state lying energetically within the GaAs CB (band gap), while $\Delta E_{\mathrm{Bi}} < 0$ (> 0) corresponds to a resonant (bound) Bi-related localised state lying energetically within the GaAs VB (band gap). The virtual crystal (conventional alloy) shifts to the CB, VB and SO band edge energies – which, by definition, are linear in the N and Bi compositions – are respectively defined as $\delta E_{\mathrm{CB}}^{\mathrm{VC}} = -\alpha_{\mathrm{Bi}}\,x - \alpha_{\mathrm{N}}\,y$, $\delta E_{\mathrm{VB}}^{\mathrm{VC}} = \kappa_{\mathrm{Bi}}\,x + \kappa_{\mathrm{N}}\,y$ and $\delta E_{\mathrm{SO}}^{\mathrm{VC}} = -\gamma_{\mathrm{Bi}}\,x - \gamma_{\mathrm{N}}\,y$. [3, 7]

The energy shifts due to the hydrostatic and axial components of the strain are given respectively by $\delta E_i^{\mathrm{hy}} = a_i(\epsilon_{xx} + \epsilon_{yy} + \epsilon_{zz})$ and $\delta E_i^{\mathrm{ax}} = -\frac{b_i}{2}(\epsilon_{xx} + \epsilon_{yy} - 2\epsilon_{zz})$, where $i =$ CB, VB, N or Bi denotes the hydrostatic and axial deformation potentials a_i and b_i associated respectively with the GaAs host matrix CB and VB edges, and with the N- and Bi-related localised states. [3, 9] We note that (i) for pseudomorphic strain, $\epsilon_{xx} = \epsilon_{yy}$ and $\epsilon_{zz} = -\frac{2C_{12}}{C_{11}}\epsilon_{xx}$, and (ii) by symmetry, $b_{\mathrm{N}} = 0$ (since the axial component of the strain has no effect on the purely s-like N-related localised states). The components of the strain tensor are determined via the mismatch between the lattice constants

TABLE S4. N- and Bi-related parameters for the 14-band Hamiltonian of $GaN_yAs_{1-x-y}Bi_x$, obtained on the basis of the tight-binding supercell calculations. In $GaAs_{1-x}Bi_x$ (GaN_yAs_{1-y}) ΔE is given relative to the unperturbed GaAs valence (conduction) band edge. Due to their A_1 symmetry, the energy of the localised states associated with isolated substitutional N impurities is not affected by axial strain: there is no associated axial deformation potential b_N.

Parameter	$GaAs_{1-x}Bi_x$	GaN_yAs_{1-y}
ΔE (eV)	-0.183	0.187
α (eV)	2.63	1.55
β (eV)	1.13	2.00
γ (eV)	0.55	-1.53
κ (eV)	1.01	1.36
a (eV)	-1.11	0.83
b (eV)	-1.71	—

$a(x,y)$ and a_S of $GaN_yAs_{1-x-y}Bi_x$ and the GaAs substrate: $\epsilon_{xx} = \frac{a_S - a(x,y)}{a_S}$. The lattice and elastic constants, and CB and VB edge deformation potentials, are determined for $GaN_yAs_{1-x-y}Bi_x$ by interpolating linearly between those of GaN, GaAs and GaBi. [3, 10, 37] The N- and Bi-related parameters of the 14-band model, derived on the basis of TB supercell calculations, [3, 7] are provided in Table S4.

For the analysis of the electronic and optical properties of QWs, the 14-band Hamiltonian is solved directly in the envelope function approximation (EFA) for each QW heterostructure using a numerically efficient reciprocal space plane wave approach. [4] The QW band structure calculations are carried out in the axial approximation. In the plane wave approach the momentum matrix elements $P^{(\widehat{e})}_{nm}(\mathbf{k}_\parallel)$ – between the QW eigenstates $|n\mathbf{k}_\parallel\sigma\rangle$ and $|m\mathbf{k}_\parallel\sigma\rangle$ at in-plane wave vector $\mathbf{k}_\parallel$ – are computed in reciprocal space using the general formulation due to Szmulowicz [4]

$$P^{(\widehat{e})}_{nm}(\mathbf{k}_\parallel) = \frac{m_0}{\hbar}\sum_{\sigma,\sigma'}\langle n\mathbf{k}_\parallel\sigma|\widehat{e}\cdot\nabla_{\mathbf{k}}\widehat{H}|m\mathbf{k}_\parallel\sigma'\rangle\,, \tag{S8}$$

where $\widehat{e}\cdot\nabla_{\mathbf{k}}\widehat{H}$ is the operator obtained by (i) taking the directional derivative of the matrix elements of the bulk $\mathbf{k}\cdot\mathbf{p}$ Hamiltonian with respect to $\mathbf{k}$ along $\widehat{e}$, and (ii) symmetrising with respect to position-dependent material parameters and quantising k_z in the usual manner. Using Eqs. (S4) and (S8) we compute the optical transition strength (in units of energy) directly for

each structure in terms of the zone-centre momentum matrix element as $\frac{2m_0}{\hbar^2}|P_{nm}^{(\widehat{e})}(0)|^2$, where $\widehat{e} = \widehat{x}$ and $\widehat{z}$ for transverse electric- (TE-) and transverse magnetic- (TM-) polarised transitions, respectively. We note that this approach to calculating the optical transition strengths directly employs the supercell Hamiltonian and computed eigenstates for a given structure, meaning that the full effects of N- and Bi-induced hybridisation are explicitly accounted for in the analysis of the optical properties. [4, 35]

Section S2: Dilute doping limit: impact of co-alloying N and Bi on the GaAs electronic structure

The interactions of individual substitutional N and Bi atoms with the host matrix states in the GaN_yAs_{1-y} and $GaAs_{1-x}Bi_x$ alloys, respectively, have been well studied in the literature. [27, 34] An isolated N atom introduces a resonant impurity state above the CB edge in GaAs [27], while an isolated Bi atom introduces a impurity state lying below the GaAs VB edge in energy. [34] However, no quantitative analysis has been undertaken to date to quantify the extent of any interaction between the localised impurity states associated with N and Bi when both are incorporated substitutionally into GaAs. Since their individual behaviours are characterized by BAC interactions in the CB and VB, it is pertinent to investigate the degree to which this behaviour remains intact in the quaternary $GaN_yAs_{1-x-y}Bi_x$ alloy. Here, we systematically analyse the interaction between these localised states by placing single substitutionaly N and Bi atoms inside a large 4096-atom $Ga_{2048}N_1As_{2046}Bi_1$ supercell, and probe the interaction as a function of the spatial separation of these impurities. We begin by placing the N and Bi atoms sufficiently far apart that the interaction between their associated localised impurity states is minimal, and then gradually bring them closer together, finally studying the case where the N and Bi atoms are located at adjacent sites on the anion sublattice (i.e. so that they are second-nearest neighbours, sharing a common Ga nearest neighbour). This latter case is that of maximum spatial overlap between the N- and Bi-related localised impurity states, and hence represents the case in which the interaction between these states would be maximised in a substitutional $GaN_yAs_{1-x-y}Bi_x$ alloy. As described in the main paper, we analyse the character of this interaction by computing the fractional GaAs Γ character of the alloy CB and VB edge states in each supercell.

Figure S1 contains schematic illustrations of the different local neighbour environments con-

sidered in this analysis. The relative positions of the N and Bi atoms in each case are defined in Sec. III A of the main text. The distinct local neighbour environments considered are (a) an unperturbed GaAs supercell, as well as a GaAs supercell containing (b) a single N impurity, (c) a single Bi impurity, and GaAs supercells in which a single Bi impurity is placed with respect to the N atom at the (d) third-closest, (e) second-closest, and (f) closest sites on the anion sub-lattice. This final case is that referred to above, whereby the N and Bi atoms are second-nearest neighbours sharing a common Ga nearest neighbour. The labelling scheme used to denote these distinct local neighbour environments is defined in Sec. III A of the main paper.

Figure S2 shows the fractional GaAs CB and VB edge Γ character $G_{\Gamma}(E)$ spectra for the ternary $Ga_{2048}N_1As_{2047}$ and $Ga_{2048}As_{2047}Bi_1$ supercells. These spectra clearly indicate hybridisation between the GaAs CB (VB) edge states and a resonant state associated with the substitutional N (Bi) atoms, lying energetically within the CB (VB) of the GaAs host matrix semiconductor. This hybridisation is the signature of the (V)BAC interactions described in Sec. S1 above, and is consistent with the established trends described in the references provided therein. For the $Ga_{2048}N_1As_{2047}$ in Fig. S2 (a) we calculate the the alloy CB edge state has 87.4% GaAs CB edge character and is shifted downwards in energy by 19 meV with respect to the unperturbed GaAs CB edge. Almost the entirety of the remainder of the GaAs CB edge character is calculated to reside on a state lying at an energy of approximately 1.64 eV, and which is highly localised about the N atomic site. We compute that the N localised resonant state if of energy 1.62 eV in this supercell – i.e. lying approximately 190 meV above the room temperature GaAs CB edge. Figure S2 (b) demonstrates that the VB edge states in $Ga_{2048}N_1As_{2047}$ are virtually unchanged compared to those in a pure $Ga_{2048}As_{2048}$ supercell, with the alloy VB edge states having $> 99.9\%$ overlap with the VB edge states of the unperturbed GaAs host matrix, reflecting that while N incorporation significantly perturbs the CB structure, its impact on the VB structure is minimal.

In Fig. S2(d) the $Ga_{2048}As_{2047}Bi_1$ supercell we observe complementary behaviour: we find that the majority ($> 96\%$) of the GaAs VB edge character resides on the alloy VB edge states, which are shifted upwards in energy compared to those in the GaAs host matrix. The remainder of the GaAs VB edge character primarily resides on a single alloy VB state, lying ~ 100 meV below the unperturbed GaAs VB edge in energy, with further smaller amounts projected onto lower lying VB states (off scale in Fig. S2 (d)). Again, this hybridisation describes the presence of BAC behaviour, this time resulting from coupling between the VB edge states of the GaAs host matrix, and impurity states that are resonant with the GaAs VB and strongly localised about the Bi

atomic site. Fig. S3 (c) highlights that the calculated overlap between the alloy CB edge state and the CB edge state of unperturbed GaAs is $> 99.9\%$, reflecting that Bi incorporation primarily impact the VB structure while having minimal impact on the CB structure.

Having understood the key trends in the ternary supercell calculations, we now turn our attention to the corresponding calculations for the quaternary $Ga_{2048}N_1As_{2046}Bi_1$ supercells containing both N and Bi, and analyse the changes in the calculated fractional GaAs CB and VB edge Γ character brought about by co-alloying N and Bi. Table I in the main text provides the band edge energies calculated for each of these supercells. Examining the fractional GaAs CB edge Γ character Figs. S3 (a), (c) and (e), we note that the trends observed in the presence of Bi remain relatively unchanged from those calculated for the ternary $Ga_{2048}N_1As_{2047}$ supercell. This indicates that the impact of N on the CB structure in $GaN_yAs_{1-x-y}Bi_x$ remains close to that in the ternary GaN_yAs_{1-y} alloy when Bi is incorporated, providing further confirmation of the trends identified in the main paper: Bi incorporation produces only minor quantitative changes to the nature of the CB structure, with the overall character remaining qualitatively unchanged, even in the case when substitutional N and Bi atoms share common Ga nearest neighbours. Turning our attention to the VB structure, we again note the same general trend: the overall character of the alloy VB edge states is qualitatively similar to that in the ternary $GaAs_{1-x}Bi_x$ alloy, with relatively minor quantitative changed brought about by co-alloying with N. The primary feature revealed by the calculated fractional GaAs VB edge Γ character in Figs. S3 (b), (d) and (f) is that the presence of N tends to lift degeneracy of the LH- and HH-like VB edge states. This effect is associated with the fact that the different local neighbour environments containing both N and Bi represent disorder alloy microstructure in which the translational symmetry of the crystal lattice is broken, leading to a breakdown of the T_d point group symmetry of the GaAs lattice. This lack of isotropy in the local crystal structure, which is compounded by the large local relaxation of the crystal lattice about complexes of spatially proximate N and Bi atoms, is then manifested in the lifting of the degeneracy of the p-like alloy VB edge states due to the associated non-equivalence of the [001], [010] and [001] crystal directions. This lifting of the VB edge energy is qualitatively identical to that we have calculated previously in disordered $GaAs_{1-x}Bi_x$ alloys, but in quantitative terms tends to be larger in magnitude in $GaN_yAs_{1-x-y}Bi_x$ due to the aforementioned large local relaxation of the crystal lattice in cases where N and Bi atoms are located close to one another.

Section S3: Electron and hole probability density plots for GaBiAs/GaAs QWs:

Here we consider the electronic structure of the N-free $GaAs_{1-x}Bi_x$/GaAs QWs having $x = 6.25$ and 9% (structures 1 and 2 of Secs. III C and III D in the main paper). Figures S5 (a) and (b) respectively show the probability density along the (001) direction, associated with the lowest energy electron state $e1$ (upper row) and highest energy hole state $h1$ (lower row) in structures 1 and 2, for five representative supercells containing distinct random distributions (RDs) of substitutional N and Bi atoms. Solid and dashed red lines respectively denote the probability density projected to cations and anions, calculated using the TB method at a fixed position z along (001) by summing over the probability density associated with all atoms in the plane perpendicular to (001). The plots from **k·p** model are shown in the Fig. 3 of the main text. Comparison of the TB and **k·p** calculations suggest that the electron states in $GaAs_{1-x}Bi_x$/GaAs QWs are broadly similar in nature to those in conventional QWs – e.g. $In_xGa_{1-x}As$/GaAs – since the electron eigenstates are (i) well described in terms of envelope functions which vary slowly and smoothly with position, (ii) effectively insensitive to the presence of underlying short-range alloy disorder, and (iii) relatively insensitive to changes in Bi composition (in this case, from $x = 6.25$ to 9% between structures 1 and 2). This is consistent with the expected behaviour for $GaAs_{1-x}Bi_x$ alloys and heterostructures: Bi incorporation strongly perturbs the VB while leaving the CB relatively unaffected, with the evolution of the latter readily captured by conventional alloy descriptions. We note also that in all supercells considered $e1$ is localised within the $GaAs_{1-x}Bi_x$ layer, reflecting the appreciable type-I $GaAs_{1-x}Bi_x$/GaAs CB offset $\Delta E_{\rm CB}$. [3, 7, 34, 35] This is confirmed by the calculated increase in the $e1$ probability density in the centre of the QW in structure 2, reflecting the increase in $\Delta E_{\rm CB}$ ($\sim -\alpha_{\rm Bi}\, x + \delta E_{\rm CB}^{\rm hy}$) brought about by increasing the Bi composition from that in structure 1.

By contrast, the $h1$ probability density (lower row, Figs. S5 (a) and (b)) calculated for structures 1 and 2 using the TB method is strongly perturbed compared to that calculated using the **k·p** method in the EFA. While the $h1$ probability density is, as expected, confined within the Bi-containing layer and primarily localised at anion sites, there is a significant departure from the smooth, envelope function-like spatial variation observed for the $e1$ eigenstates. In contrast to the probability density associated with $e1$, which is spread across the extent of the QW, for $h1$ we observe extremely strong localisation of the probability density at various different locations within the QW, with strong dependence of this localisation on the precise short-range alloy

disorder present in the QW. We have previously identified that this unusual behaviour has its origins in Bi-related alloy disorder, specifically in the formation of pairs and larger clusters of Bi atoms in a realistic $GaAs_{1-x}Bi_x$ alloy. [33] As described above, these pairs and clusters create a full distribution of localised states lying close in energy to the VB edge, which then hybridise strongly with extended GaAs VB states leading to a multiplicity of VB edge states having significant localised character (low Bloch character). Further analysis reveals that this strong spatial localisation of the hole eigenstates typically occurs about the largest Bi clusters present in a given alloy (reflected here in the sense that a large TB calculated probability density reflects the presence of Bi pairs and/or clusters in the plane at that value of z). The precise distribution of Bi-related localised states depends closely on the precise short-range alloy disorder present in the $GaAs_{1-x}Bi_x$ layers in these QW structures, thereby accounting for the observed strong variation of the localisation of the $h1$ eigenstates at fixed compositions for structures containing different RDs of Bi atoms. Comparing the $h1$ probability density from the TB calculations with that obtained using the 14-band $\mathbf{k}\cdot\mathbf{p}$ model in the EFA (shown in Fig. 4 of the main paper), we conclude that (i) the strongly perturbative impact of Bi incorporation and alloy disorder on the VB structure in $GaAs_{1-x}Bi_x$ leads to a strong breakdown of the envelope function description of the hole eigenstates in $GaAs_{1-x}Bi_x$/GaAs heterostructures, and (ii) this breakdown of the EFA for hole eigenstates is a generic feature of the electronic properties $GaAs_{1-x}Bi_x$/GaAs in the sense that it is intrinsic and effectively insensitive to the Bi composition.

Section S4: Probability densities in $GaN_yAs_{1-x-y}Bi_x$/GaAs quantum wells

In the main paper we present probability densities calculated for the same 8 nm thick $GaN_{0.025}As_{0.9125}Bi_{0.0625}$/GaAs and $GaN_{0.01}As_{0.90}Bi_{0.09}$/GaAs QWs (structures 3 and 4, respectively) using the TB method, for selected supercells containing distinct RDs of N and Bi atoms substituted on the anion sublattice in the well region (cf. Fig. S4). Figures S6 (a) and (b) respectively present probability densities calculated for these two QWs, for several additional RDs in each case. The line types are as in Fig. 2 of the main paper. The calculated trends are qualitatively similar here to those discussed for the other RDs in the main paper and, as such, we refer the reader to Sec. III C of the main paper for a discussion of the associated trends.

[1] K. Alberi, J. Wu, W. Walukiewicz, K. M. Yu, O. D. Dubon, S. P. Watkinsa, C. X. Wang, X. Liu, Y.-J. Cho, and J. Furdyna, Valence-band anticrossing in mismatched iii-v semiconductor alloys, Phys. Rev. B 75, 045203 (2007).

[2] Z. Batool, K. Hild, T. J. C. Hosea, X. Lu, T. Tiedje, and S. J. Sweeney, The electronic band structure of GaBiAs/GaAs layers: Influence of strain and band anti-crossing, J. Appl. Phys. 111, 113108 (2012).

[3] C. A. Broderick, P. E. Harnedy, P. Ludewig, Z. L. Bushell, K. Volz, R. J. Manning, and E. P. O'Reilly, Determination of type-I band offsets in $GaBi_xAs_{1-x}$ quantum wells using polarisation-resolved photovoltage measurements and 12-band $\mathbf{k}\cdot\mathbf{p}$ calculations, Semicond. Sci. Technol. 30, 094009 (2015).

[4] C. A. Broderick, P. E. Harnedy, and E. P. O'Reilly, Theory of the electronic and optical properties of dilute bismide quantum well lasers, IEEE J. Sel. Top. Quant. Electron. 21, 1503313 (2015).

[5] C. A. Broderick, I. P. Marko, E. P. O'Reilly, and S. J. Sweeney, "Dilute Bismide Alloys", Chapter 10 – Handbook of Optoelectronic Device Modeling and Simulation (Vol. 1), in press, 2017.

[6] C. A. Broderick, S. Mazzucato, H. Carrère, T. Amand, H. Makhloufi, A. Arnoult, C. Fontaine, O. Donmez, A. Erol, M. Usman, E. P. O'Reilly, and X. Marie, Anisotropic electron g factor as a probe of the electronic structure of $GaBi_xAs_{1-x}$/GaAs epilayers, Phys. Rev. B 90, 195301 (2014).

[7] C. A. Broderick, M. Usman, and E. P. O'Reilly, Derivation of 12 and 14-band $\mathbf{k}\cdot\mathbf{p}$ hamiltonians for dilute bismide and bismide-nitride alloys, Semicond. Sci. Technol. 28, 125025 (2013).

[8] C. A. Broderick, M. Usman, S. J. Sweeney, and E. P. O'Reilly, Band engineering in dilute nitride and bismide semiconductor lasers, Semicond. Sci. Technol. 27, 094011 (2012).

[9] G. M. T. Chai, C. A. Broderick, S. R. Jin, J. P. Petropoulous, Y. Zhong, P. B. Dongmo, J. M. O. Zide, E. P. O'Reilly, S. J. Sweeney, and T. J. C. Hosea, Experimental and modelling study of InGaBiAs/InP alloys with up to 5.8% Bi, and with $\Delta_{\mathrm{SO}} > E_g$, Semicond. Sci. Technol. 30, 094015 (2015).

[10] M. Ferhat and A. Zaoui, Structural and electronic properties of iii-v bismuth compounds, Phys. Rev. B 73, 115107 (2006).

[11] B. Fluegel, S. Francoeur, A. Mascarenhas, S. Tixier, E. C. Young, and T. Tiedje, Giant spin-orbit bowing in $GaAs_{1-x}Bi_x$, Phys. Rev. Lett. 97, 067205 (2006).

[12] A. Janotti, S.-H. Wei, and S. B. Zhang, Theoretical study of the effects of isovalent coalloying of Bi and N in GaAs, Phys. Rev. B 65, 115203 (2002).

[13] P. N. Keating, Effect of invariance requirements on the elastic strain energy of crystals with application to the diamond structure, Phys. Rev. 145, 637 (1966).

[14] P. R. C. Kent, L. Bellaiche, and A. Zunger, Pseudopotential theory of dilute IIIV nitrides, Semicond. Sci. Technol. 17, 851 (2002).

[15] P. R. C. Kent and A. Zunger, Evolution of III-V nitride alloy electronic structure: the localized to delocalized transition, Phys. Rev. Lett. 86, 2613 (2001).

[16] P. R. C. Kent and A. Zunger, Theory of electronic structure evolution in GaAsN and GaPN alloys, Phys. Rev. B 64, 115208 (2001).

[17] G. Klimeck, S. S. Ahmed, H. Bae, N. Kharche, R. Rahman, S. Clark, B. Haley, S. Lee, M. Naumov, H. Ryu, F. Saied, M. Prada, M. Korkusinski, and T. Boykin, Atomistic simulation of realistically sized nanodevices using NEMO 3-D – part I: models and benchmarks, IEEE Trans. Electron. Dev. 54, 2079 (2007).

[18] G. Klimeck, S. S. Ahmed, N. Kharche, M. Korkusinski, M. Usman, M. Prada, and T. Boykin, Atomistic simulation of realistically sized nanodevices using NEMO 3-D – part II: applications, IEEE Trans. Electron. Dev. 54, 2090 (2007).

[19] O. L. Lazarenkova, P. von Allmen, F. Oyafuso, S. Lee, and G. Klimeck, Effect of anharmonicity of the strain energy on band offsets in semiconductor nanostructures, Appl. Phys. Lett. 85, 4193 (2004).

[20] A. Lindsay, The theory of the electronic structure of GaN_xAs_{1-x} and $In_yGa_{1-y}N_xAs_{1-x}$, PhD thesis, University of Surrey, 2002.

[21] A. Lindsay and E. P. O'Reilly, Influence of nitrogen resonant states on the electronic structure of GaN_xAs_{1-x}, Solid State Commun. 118, 313 (2001).

[22] A. Lindsay and E. P. O'Reilly, A universal model for trends in a_1-type defect states in zincblende and diamond semiconductor structures, Physica B 434, 340 (2003).

[23] A. Lindsay and E. P. O'Reilly, Unification of the band anticrossing and cluster-state models of dilute nitride semiconductor alloys, Phys. Rev. Lett. 93, 196402 (2004).

[24] A. Lindsay, S. Tomić, and E. P. O'Reilly, Derivation of a 10-band $\mathbf{k}\cdot\mathbf{p}$ model for dilute nitride semiconductors, Solid State Electron. 47, 443 (2003).

[25] E. P. O'Reilly and A. Lindsay, Tight-binding approach to calculation of localised perturbations in

semiconductors, J. Phys.: Conf. Ser. 242, 012002 (2010).

[26] E. P. O'Reilly, A. Lindsay, and S. Fahy, Theory of the electronic structure of dilute nitride alloys: beyond the band-anti-crossing model, J. Phys. Condens. Matter 16, S3257 (2004).

[27] E. P. O'Reilly, A. Lindsay, P. J. Klar, A. Polimeni, and M. Capizzi, Trends in the electronic structure of dilute nitride alloys, Semicond. Sci. Technol. 24, 033001 (2009).

[28] E. P. O'Reilly, A. Lindsay, S. Tomić, and M. Kamal-Saadi, Tight-binding and $\mathbf{k}\cdot\mathbf{p}$ models for the electronic structure of Ga(In)NAs and related alloys, Semicond. Sci. Technol. 17, 870 (2002).

[29] W. Shan, W. Walukiewicz, J. W. Ager III, E. E. Haller, J. F. Geisz, D. H. Friedman, J. M. Olson, and S. R. Kurtz, Band anticrossing in GaInNAs alloys, Phys. Rev. Lett. 82, 1221 (1999).

[30] N. Shtinkov, P. Desjardins, and R. A. Masut, Empirical tight-binding model for the electronic structure of dilute GaNAs alloys, Phys. Rev. B 67, 081202(R) (2003).

[31] J. C. Slater and G. F. Koster, Simplified LCAO method for the periodic potential problem, Phys. Rev. 94, 1498 (1954).

[32] S. Tomić, E. P. O'Reilly, R. Fehse, S. J. Sweeney, A. R. Adams, A. D. Andreev, S. A. Choulis, T. J. C. Hosea, and H. Riechert, Theoretical and experimental analysis of 1.3-μm InGaNAs/GaAs lasers, IEEE. J. Sel. Top. Quantum Electron. 9, 1228 (2003).

[33] M. Usman, C. A. Broderick, Z. Batool, K. Hild, T. J. C. Hosea, S. J. Sweeney, and E. P. O'Reilly, Impact of alloy disorder on the band structure of compressively strained $GaBi_xAs_{1-x}$, Phys. Rev. B 87, 115104 (2013).

[34] M. Usman, C. A. Broderick, A. Lindsay, and E. P. O'Reilly, Tight-binding analysis of the electronic structure of dilute bismide alloys of GaP and GaAs, Phys. Rev. B 84, 245202 (2011).

[35] M. Usman and E. P. O'Reilly, Atomistic tight-binding study of the electronic structure and interband optical transitions in $GaBi_xAs_{1-x}$/GaAs quantum wells, Appl. Phys. Lett. 104, 071103 (2014).

[36] P. Vogl, H. P. Hjalmarson, and J. D. Dow, A semi-empirical tight-binding theory of the electronic structure of semiconductors, J. Phys. Chem. Solids 44, 365 (1983).

[37] I. Vurgaftman and J. R. Meyer, Band parameters for nitrogen-containing semiconductors, J. Appl. Phys. 94, 3675 (2003).

[38] S.-H. Wei and A. Zunger, Giant and composition-dependent optical bowing coefficient in GaAsN alloys, Phys. Rev. Lett. 76, 664 (1996).

[39] Y. Zhang, A. Mascarenhas, and L.-W. Wang, Similar and dissimilar aspects of III-V semiconductors containing Bi versus N, Phys. Rev. B 71, 155201 (2005).

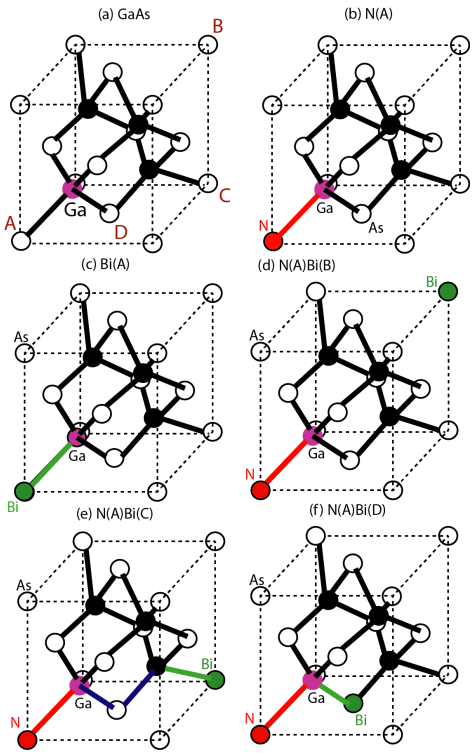

FIG. S1. Schematic illustration of a single, simple cubic 8-atom GaAs unit cell within the 4096 atom supercells considered. N and Bi atoms are substituted at specific As sites A, B, C and D on the anion sublattice (Ga and As atoms depicted respectively in black and white). (a) A pure $Ga_{2048}As_{2048}$ supercell, with the location of the anion lattice sites A – D indicated. (b) A $Ga_{2048}N_1As_{2047}$ supercell containing an isolated substitutional N impurity (depicted in red) at the anion lattice site A (denoted by GaAs:N_A). (c) A $Ga_{2048}As_{2047}Bi_1$ supercell containing an isolated substitutional Bi impurity (depicted in green) at the anion lattice site A (denoted by GaAs:Bi_A). (d) A $Ga_{2048}N_1As_{2046}Bi_1$ supercell containing single substitutional N and Bi impurities at the respective anion lattice sites A and B (denoted by GaAs:N_ABi_B), so that the N and Bi atoms are third-nearest neighbours. (e) A $Ga_{2048}N_1As_{2046}Bi_1$ supercell containing single substitutional N and Bi impurities at the respective anion lattice sites A and C (denoted by GaAs:N_ABi_C), so that the N and Bi atoms are second-nearest neighbours. (f) A $Ga_{2048}N_1As_{2046}Bi_1$ supercell containing single substitutional N and Bi impurities at the respective anion lattice sites A and D (denoted by GaAs:N_ABi_D), so that the N and Bi atoms are second-nearest neighbours.

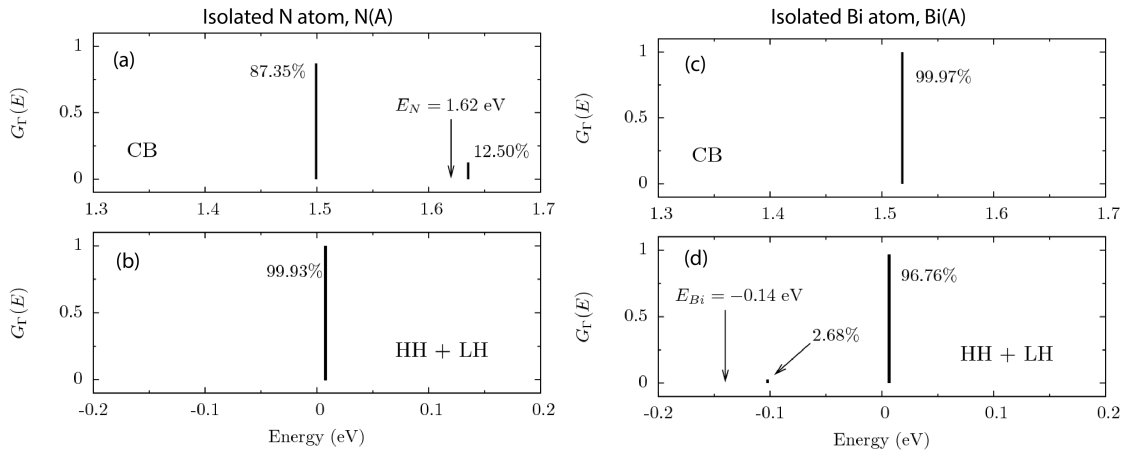

FIG. S2. Calculated GaAs fractional Γ character spectra $G_\Gamma(E)$ for the CB and VB edge states in ordered 4096-atom $Ga_{2048}N_1As_{2047}$ and $Ga_{2048}As_{2047}Bi_1$ supercells. (a) and (b) show $G_\Gamma(E)$ associated respectively with the GaAs CB and VB (i.e. combined LH and HH) edge states in $Ga_{2048}N_1As_{2047}$. (c) and (d) show $G_\Gamma(E)$ associated respectively with the GaAs CB and VB edge states in $Ga_{2048}As_{2047}Bi_1$. Band-anticrossing interactions associated with N- (Bi-) related localised resonant states are clearly visible in $G_\Gamma(E)$ calculated for the $Ga_{2048}N_1As_{2047}$ CB ($Ga_{2048}As_{2047}Bi_1$ VB), consistent with our previous calculations in Refs. [21] and [34].

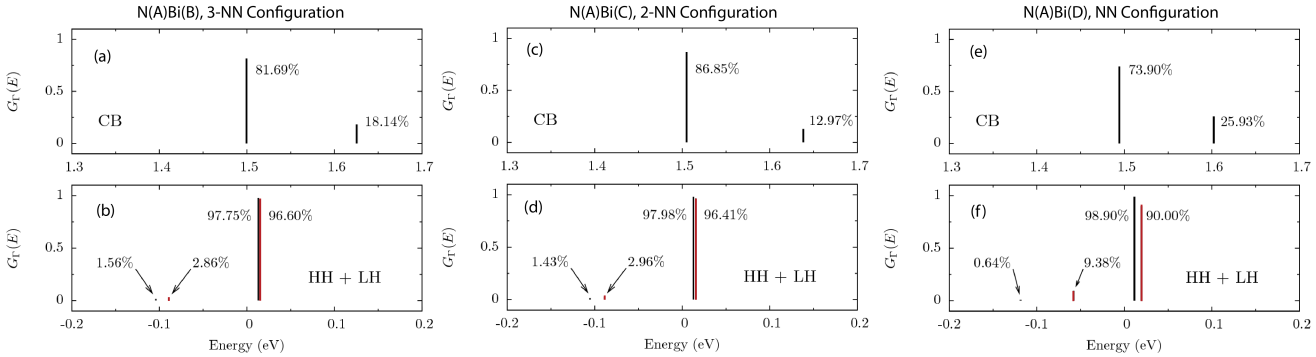

FIG. S3. Calculated GaAs fractional Γ character spectra $G_\Gamma(E)$ for the CB and VB edge states in 4096-atom $Ga_{2048}N_1As_{2046}Bi_1$ supercells containing one N and one Bi impurity arranged in different local configurations (cf. Fig. S1). (a) and (b) show $G_\Gamma(E)$ associated respectively with the GaAs CB and VB (i.e. combined LH and HH) edge states in the GaAs:N_ABi_B supercell. (a) and (b), (c) and (d), and (e) and (f) show, respectively, $G_\Gamma(E)$ associated respectively with the GaAs CB and VB (i.e. combined HH and LH) edge states in the GaAs:N_ABi_B, GaAs:N_ABi_C, and GaAs:N_ABi_D supercells. In moving the Bi atom from the I to E to B anion lattice site (cf. Fig. S1 the Bi atom is brought closer to the N atom at anion site A. The reduced symmetry in these supercells lifts the degeneracy of the LH- and HH-like Bi-related and VB edge states, with the energy splitting between these states increasing as the Bi atom is brought closer to the N site, due to larger local relaxation of the crystal lattice.

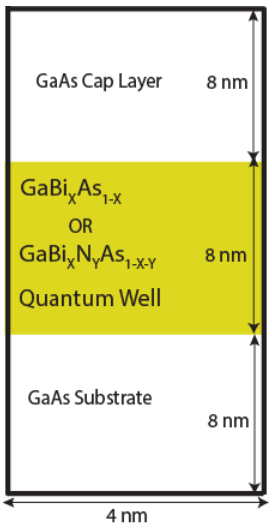

FIG. S4. Schematic illustration of the structures considered in the analysis of the electronic and optical properties of $GaN_yAs_{1-x-y}Bi_x$/GaAs quantum wells. We consider an 8 nm thick quantum well surrounded by 8 nm thick GaAs barriers, giving a total length of 24 nm along the (001) growth direction and a separation of 16 nm between image quantum wells associated with the Born von Karman boundary conditions. The lateral dimensions are taken to be 4 nm along the (100) and (010) in-plane directions. In the tight-binding calculations this corresponds to a supercell of volume 384 nm^3 containing a total of 24,576 atoms. The same geometry along (001) is employed in the 14-band $\mathbf{k}\cdot\mathbf{p}$ calculations with the exception that the calculation proceeds in one dimension only, so that the lateral dimensions are inconsequential.

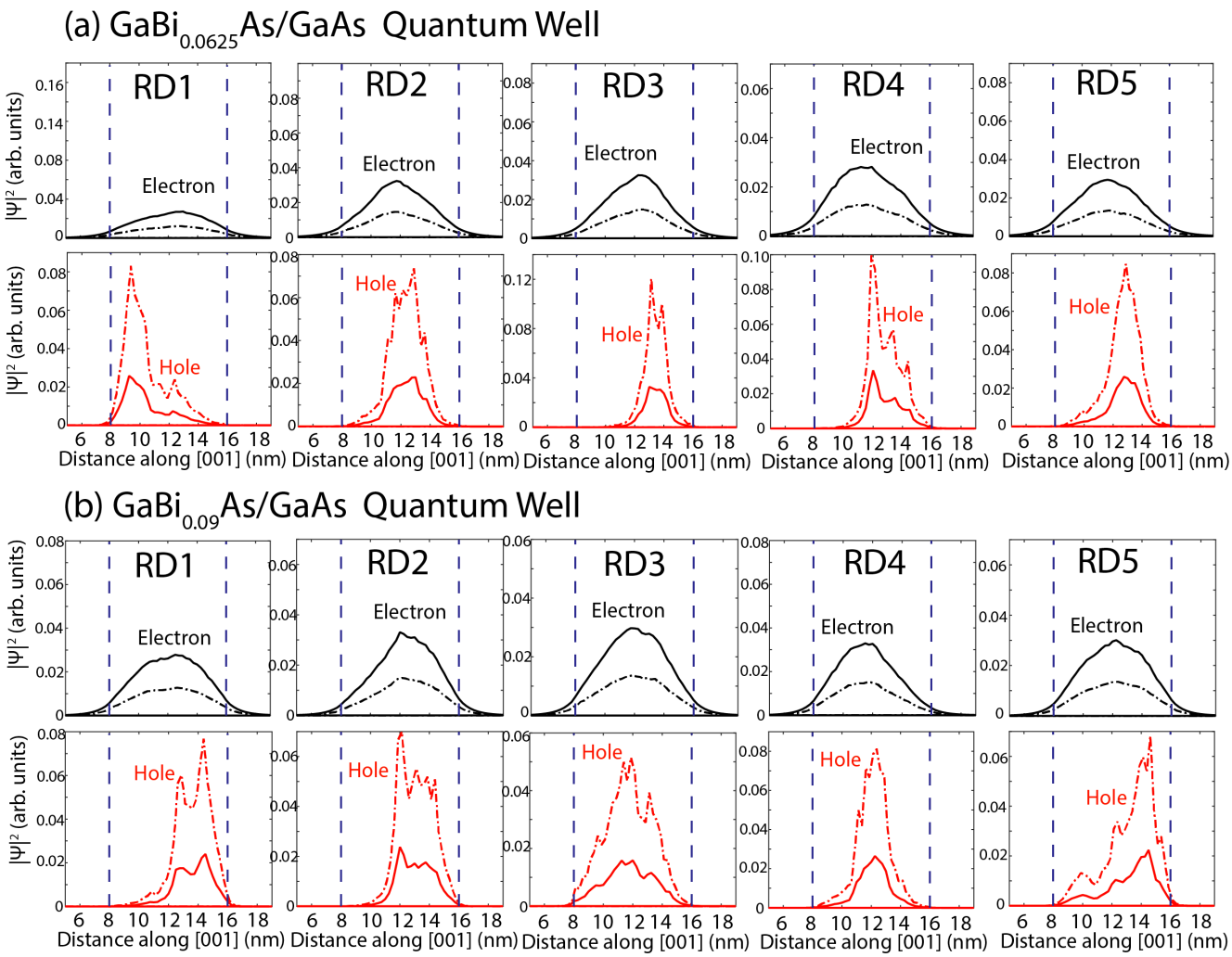

FIG. S5. Probability density associated with the lowest energy conduction electron state (upper row) and highest energy valence hole state (lower row) in N-free (a) $GaAs_{0.9375}Bi_{0.0625}/GaAs$ ($x = 6.25\%$), and (b) $GaAs_{0.91}Bi_{0.09}/GaAs$ ($x = 9\%$) quantum wells (cf. Fig. S4). Solid (dash-dotted) black lines and solid (dash-dotted) red lines show, respectively, the electron and hole probability density at cation (anion) sites calculated using the sp^3s^* tight-binding model, obtained at each position z along the growth direction by summing over the probability densities associated with each atom in the plane. Vertical dashed black lines denote the well/barrier interfaces. The tight-binding calculations were performed for five different random distributions (RDs), corresponding to structures with fixed x and y in which the N and Bi atoms were substituted at randomly selected sites on the anion sublattice. It can be seen clearly that Bi-related alloy disorder strongly perturbs the VB leading to strong hole localisation, but that the CB is relatively unaffected with the electron probability densities retaining the smooth envelope function-like behaviour.

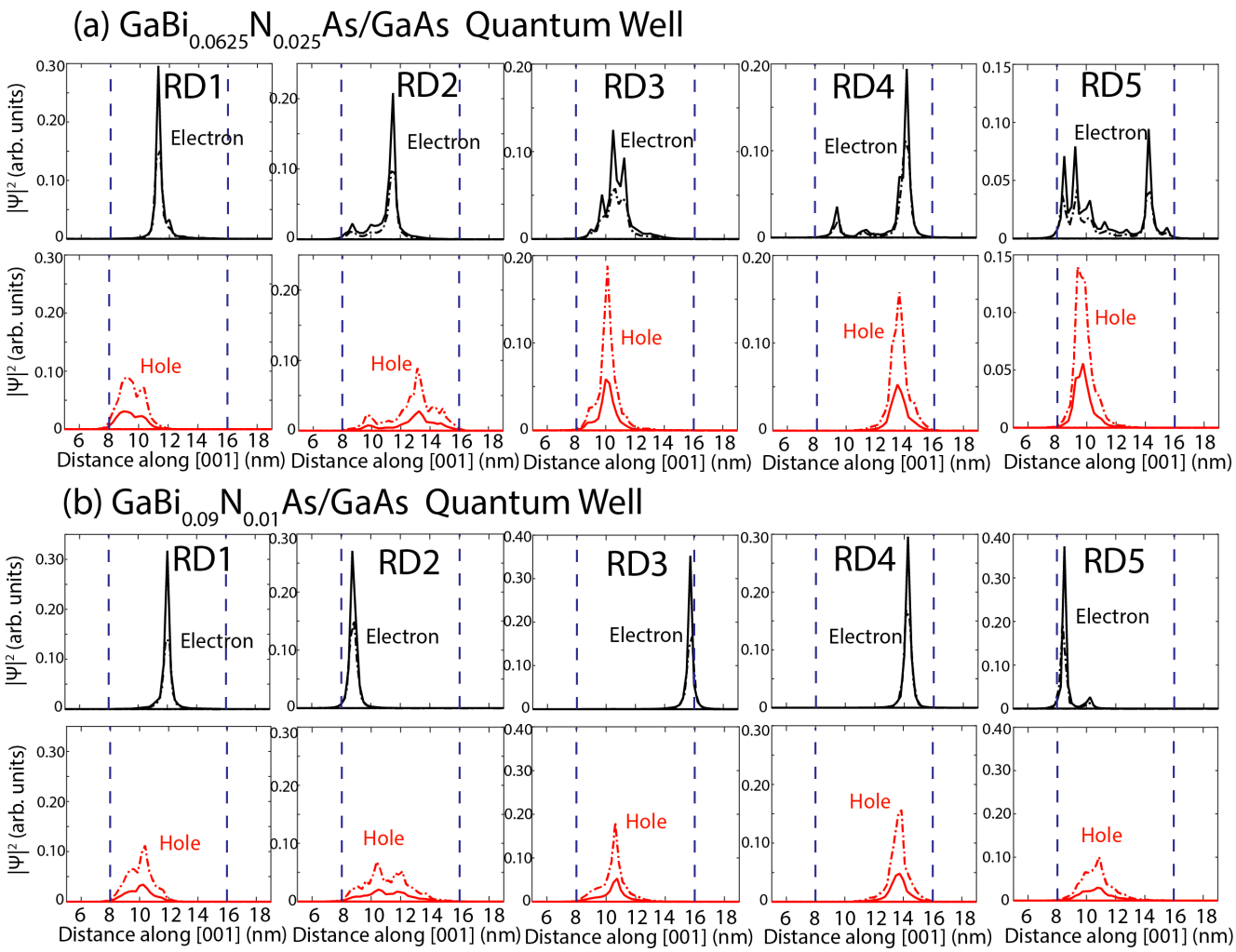

FIG. S6. Probability density associated with the lowest energy CB electron state ($e1$; upper row) and highest energy VB hole state ($h1$; lower row) in 8 nm thick (a) $GaN_{0.025}As_{0.9125}Bi_{0.0625}/GaAs$ ($x = 6.25\%$, $y = 2.5\%$), and (b) $GaN_{0.01}As_{0.90}Bi_{0.09}/GaAs$ ($x = 9\%$, $y = 1\%$) QWs. Solid (dash-dotted) black lines and solid (dash-dotted) red lines respectively denote the $e1$ and $h1$ probability density at cation (anion) sites calculated using the TB model, obtained at each position z along the [001] growth direction by summing over the probability densities associated with each atom in the plane. Dashed blue lines denote the well/barrier interfaces. The TB calculations were performed for five supercells containing different random spatial distributions (RDs) of substitutional N and Bi atoms on the anion sublattice.